Ibn Al-Haitham Journal for Pure and Applied Sciences
Journal homepage: jih.uobaghdad.edu.iq
PISSN: 1609-4042, EISSN: 2521-3407
IHJPAS. 2025, 38(4)

Green Synthesis and characterization of the ZnO, CuO and ZnO@CuO, Nanoparticles for antibacterial activity

Alzahraa Fadhel Alzidi[1] and Eman M. Nasir[2*]
[1]Department of Physics, College of Science for women, University of Baghdad, Baghdad, Iraq
[2]Department of Physics, College of Science, University of Baghdad, Baghdad, Iraq
*Corresponding Author.

Received: 20 March 2025 Accepted: 24 July 2025 Published: 20 October 2025
doi.org/10.30526/38.4.4141

Abstract

In this study, an extract from bamboo leaves was used to prepare ZnO NPs, CuO NPs, and ZnO/CuO NPs in a safe, efficient, and eco-friendly manner to reduce the toxicity of nanomaterials and their use in medical applications. XRD analysis confirmed the crystalline nature of the synthesized nanoparticles. The average crystalline size was 22 nm for ZnO, 13.8 nm for CuO, and 14.7 nm for the CuO-ZnO composite. ZnO nanoparticles were hexagonal, while CuO nanoparticles were monoclinic. FESEM demonstrated that the produced nanoparticles were formed in various configurations, combining spherical flower shapes with nanorods with sizes ranging from 30 to 60 nm, which promotes the creation of images and nanoparticles. EDX analysis verified that all samples contained the elements that were present (O, Zn, and Cu). UV-Vis was used to calculate the ZnO, CuO, and ZnO/CuO energy gaps are 4.2 eV, 3.08 eV, and (3.26, 3.72) eV, respectively. Additionally, the investigation found that the extract from bamboo leaves included functional groups that serve as agents that reduce and cap. Furthermore, ZnO NPs, CuO NPs, and ZnO/CuO nanocomposites showed great stability at 76.8, 57.2, and 71.6, respectively, according to zeta potential. The study revealed that the material demonstrates greater antibacterial activity against Gram-negative bacteria compared to Gram-positive ones.

Keywords: Bamboo leaf extract, Biomedical application, ZnO/CuO nanocomposite, Green synthesis, Nanoflower.

1.Introduction

Nanotechnology encompasses scientific and engineering disciplines that focus on phenomena at the nanoscale. It involves the creation, characterization, production, and use of materials and systems with unique properties. The concept was first introduced in 1959 by Richard Feynman, a physicist who proposed the idea of building materials and devices on atomic and molecular scales through a pioneering presentation (1). Nanotechnology has revolutionized the fields of health care and materials, and its main innovation is nanoparticles, which are one-dimensional in the range of (1-100) nanometers (2). The biological approach to the preparation of nanoparticles has gained great importance for its safety and environmental friendliness, and its dependence on natural covering and reducing agents, and producing diverse and stable nanoparticles in mild conditions without emitting

toxic by-products (3). Among the biological pathways, extracts are widely used to prepare nanoparticles and avoid harmful chemicals and their associated toxic effects (4).

The study of nanomaterials has grown exponentially due to their distinctive properties, such as hardness, chemical stability, electrical conductivity, catalytic efficiency, and anti-microbial activity. They are widely used in medicine and biology to address challenges such as environmental pollution and disease spread. Nanoparticles play a vital role in creating a sustainable ecosystem, as nanotechnology has recently contributed to drug development, disease control, and improved global health (5). Metal oxide nanoparticles play a significant role in nanotechnology, as they are widely used in various industries and act as disinfectants, catalysts, and antibacterial agents, where their interaction with microbes varies depending on their size, which affects their antimicrobial efficacy (6, 7). Inorganic ones are distinctive and attractive due to their chemical stability, safety, and strong antibacterial activity (8).

They have been found in various fields such as sensors, photocatalysis, drug delivery, cosmetics, and UV protection, also as bactericidals (9). ZnO is an II-VI n-type material with a significant exciton binding energy (60 meV), optical transparency, and an Eg of 3.3 eV at ambient temperature (1). When compared to other widely used wide-band-gap materials, the properties of ZnO with a straight band gap and high exciton binding energy are significantly better. Intriguing features include its high chemical stability, eco-friendliness, affordability, availability, and non-toxicity in reducing environments (11).On the other hand, copper oxide (CuO) nanoparticles are semiconductors with a narrow energy gap of approximately 1.2 eV, chemically stable and environmentally friendly, are the basis for many high-temperature superconductors, and have the potential to reduce inflammation and bacterial activity (12).

ZnO/CuO are among the most common particles because they have outstanding physical, chemical, and mechanical properties such as large surface area, low melting point, structural stability, and high surface energy (13). There are many research studies to prepare ZnO (14) and CuO (15) as well as ZnO/CuO composites (16). The biological method and technology have several advantages over physical and chemical processes. Bamboo leaves were chosen due to their high phytochemical content (17). This study aims to prepare ZnO NPs, CuO NPs, and ZnO/CuO NPs in an environmentally friendly way using bamboo leaf extract. The research also aims to evaluate the efficiency of these nanoparticles as effective and innovative compounds in environmental and medical applications, with a focus on sustainable alternatives for the preparation of nanomaterials.

2. Materials and Methods

2.1. Plant collection and extract preparation

The leaves were cleaned three times with water and then again with deionised water (DI) to remove dust. Then dried for 3 weeks in the shade at room temperature, 10 g of leaf powder was mixed with 100 mL of DI and heated to 35°C for 1 hour, then the temperature was increased to 80°C for 1 hour. The filtered solution was then stored away from light to be used.

2.2. Preparation of ZnO NPs and CuO NPs

To synthesize ZnO NPs, 2.8756 g of zinc sulfate hydrate ($ZnSO_4 7H_2O$) was accurately weighed and dissolved in 50 mL of DI. The solution was then stirred for 30 minutes at 35°C with a stirring speed of 1100 rpm, and 15 ml of bamboo extract was added dropwise to the solution while stirring continued. The temperature was gradually increased to 60°C. The solution's color changed to a yellowish-white. After approximately 30 min, a sodium hydroxide solution was carefully added dropwise until the pH of the solution reached 12. The

solution's appearance transitioned from slightly cloudy transparent white to a milky white color. The solution was left overnight, then the precipitate was produced using centrifugation. The precipitate was washed three times with (DI) and ethanol, then dried in an oven at 80°C for 2 hours. The dried product was subjected to calcination at 550°C for one hour. To synthesize CuO NPs, use the same steps that were used to prepare ZnO NPs, a form of copper sulfate pentahydrate ($CuSO_4.5H_2O$).

2.3. Preparation of ZnO/CuO nanocomposite

Zinc sulfate hydrate (2.8756 g) and copper sulfate pentahydrate (2.49 g) were separately dissolved in 50 mL of DI and were stirred for 30 min at a temperature of 35°C with a stirring speed of 1100 rpm. Copper sulfate 2.49 g was dissolved in 50 mL of DI. The solution was stirred at 35°C for 30 min with a stirring speed of 1100 rpm (blue color). The first solution was mixed with the second solution. The bamboo leaf extract (30 ml) was added after 10 min in the form of drops, and the solution became greenish-blue in color. Sodium hydroxide was added after 30 min in drops until the pH reached 11.7, and the color of the solution turned light green. The solution was overnight and then centrifuged to collect the precipitate. The precipitate was washed three times with (DI) and ethanol and then dried in an oven at 80°C for two hours. Finally, the dried product was calcined at 550°C for one hour.

3. Results and Discussion

3.1. X-ray diffraction (XRD) analysis

X-ray diffraction (XRD) analysis of ZnO NPs is displayed in **Figure 1**. Sharp peaks in the figure show that ZnO is extremely polycrystalline. And the dominant peaks at 2 theta are 31.7, 34.3, 36.1, 47.4, 56.5, 62.8, 66.3, 67.8, and 68.9, which have a hexagonal structure and belong to the crystalline planes ((100) (002) (101) (102),(110) (103) (200) (112) (201)), respectively. The results are in good agreement with the JCPDS 01-079-0207 data (18).**Figure 1** also shows the XRD of CuO NPs polycrystalline, and the peaks at 2 theta are 32.4, 35.4, 36.3, 48.7, 53.5, 58.2, 61.49, 67.26, 67.9, 72.1, and 74.97. The corresponding diffraction angles are indicated by the Miller indices (110), (002), (111), (-202), (020), (202), (-113), (-311), (113), (311), (004), respectively. Accordingly, the strongest diffraction angles were 2 theta 35.4 and 37.4. The peaks in the diffraction pattern of CuO NPs were aligned with the standard data from card 00-005-0661. JCPDS. This demonstrates the evolution of the monoclinic crystal structure (19).

Moreover, the figure does not show any impurities, indicating that the material was formed in excellent purity. As a result, the CuO/ZnO nanocomposite's diffraction peaks show a notable and suitable integration of both metal oxide nanoparticles. Additionally, as **Figure 1** illustrates, ZnO-corresponding peak intensities in the ZnO/CuO diffraction pattern were found to be greater than CuO nanoparticle (NP) intensities. This finding points to a higher percentage of ZnO NPs with a bimetallic structure and higher crystallinity (20). The average crystalline size was determined using the Debye-Scherrer **Equation 1** (21).

$$D\ (nm) = 0.9\ \lambda / \beta\cos\theta, \quad (1)$$

Where λ is the wavelength with CuKα radiation sources (λ = 0.15417 nm), θ is the Bragg diffraction angle, and β indicates the diffraction peaks' full width at half maximum (FWHM) as calculated from XRD patterns. The average crystal sizes of ZnO NPs, CuO NPs, and ZnO/CuO nanocomposites were determined to be 22 nm, 13.8 nm, and 14.7 nm, respectively as shown in **Table 1.**

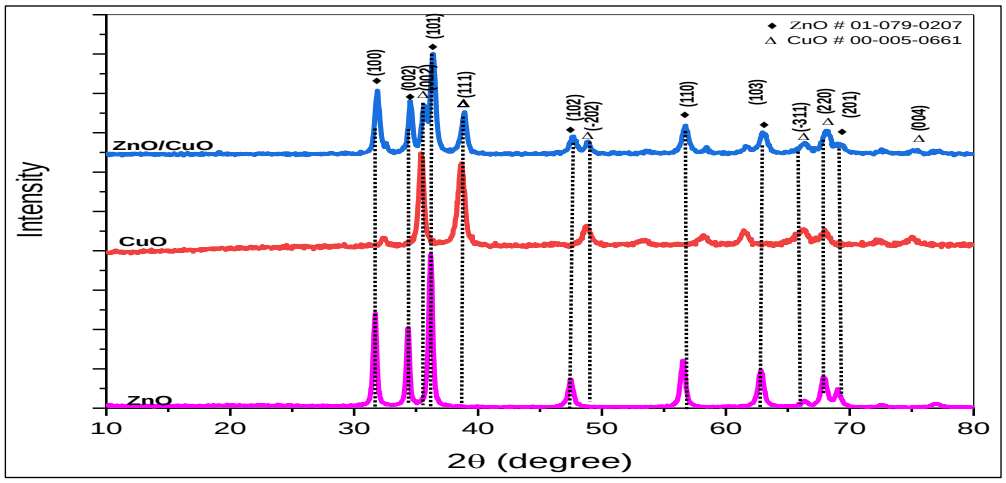

Figure 1. XRD of ZnO NPs, CuO NPs,and ZnO/CuO NCs.

Table 1. Determination of the crystalline size and structural parameters of ZnO NPs, CuO NPs and ZnO/CuO NCs.

Sample	Miller indices (hkl)	2θ (degree)	FWHM (degree)	Crystallite size D (nm)
ZnO	(100)	31.68785	0.38165	21.62
ZnO	(002)	34.35026	0.34461	24.12
ZnO	(101)	36.17216	0.41204	20.27
ZnO	(102)	47.48544	0.51929	16.70
Average crystalline size D				22 nm
CuO	(002)	35.42644	0.52066	16.01
CuO	(111)	38.64201	0.7157	11.75
Average crystalline size D				13.8 nm
ZnO/CuO	(100)	31.87707	0.49969	16.52
ZnO/CuO	(002)	34.55483	0.45057	18.45
ZnO/CuO	(101)	36.25319	0.98287	8.50
ZnO/CuO	(200)	38.86241	0.54359	15.49
Average crystalline size D				14.7 nm

3.2. Field emission scanning electron microscopy, (FE-SEM)

Field emission scanning electron microscopy, (FE-SEM) was used to detect the surface morphology of ZnO NPs, CuO NPs, and ZnO/CuO NCs, as seen in **Figures 2** (a and b), ZnO NPs in two shapes. For example, it exhibits a cluster of semi-spherical granules arranged in a flower shape, as well as particles that appear in nanorods with an average diameter of 52 nm. This result is in agreement with the research (22). In the case of CuO NPs, **Figure 2** (b and c), as seen in image (b), the particles have a semi-spherical shape and are grouped in clusters with an average diameter of 58 nm. In addition, the synthesized CuO NPs aggregated due to their high surface energy,tension, area, contact, viscous plant extract, and metal oxide nanoparticle attraction and oxidation (23). Therefore, CuO NPs attach with a high affinity to form asymmetric clusters that are rough and nearly spherical. As a result of physical interaction, ZnO/CuO NCs appear to be clustered together in irregular clusters of different sizes and shapes with an average diameter of 50 nm , indicating a significant interaction between the two compounds, as shown in **Figures 2** (e and f) (24).

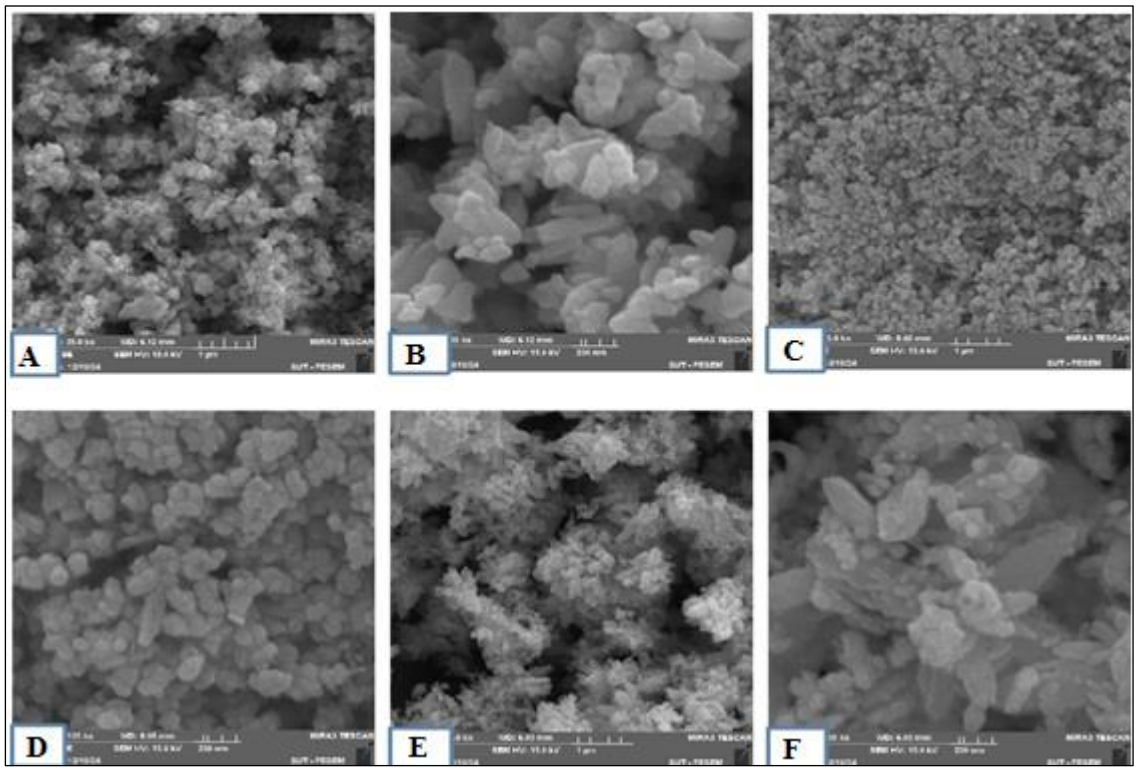

Figure 2. FE-SEM image of (**A, B**) ZnO NPs, (**C, D**) CuO NPs, (**E, F**) ZnO/CuO NCs.

3.3. Energy Dispersive X-ray (EDX) Analysis

The characterization of Energy Dispersive X-ray Spectroscopy (EDX) results is shown in **Figure 3,** which shows that the samples are very pure and that there is very little evidence of contamination from other substances during synthesis or handling. These contaminants may be impurities from equipment, feedstocks, or solvents. Theoretically, the expected equivalent mass percentage of ZnO (Zn 54.4%, O 44.2%) (24), while CuO (Cu 45.2%, O 53.88%) (25, 26), or ZnO/CuO (Cu 16.26%, Zn 39.16%, and O 44.58%).

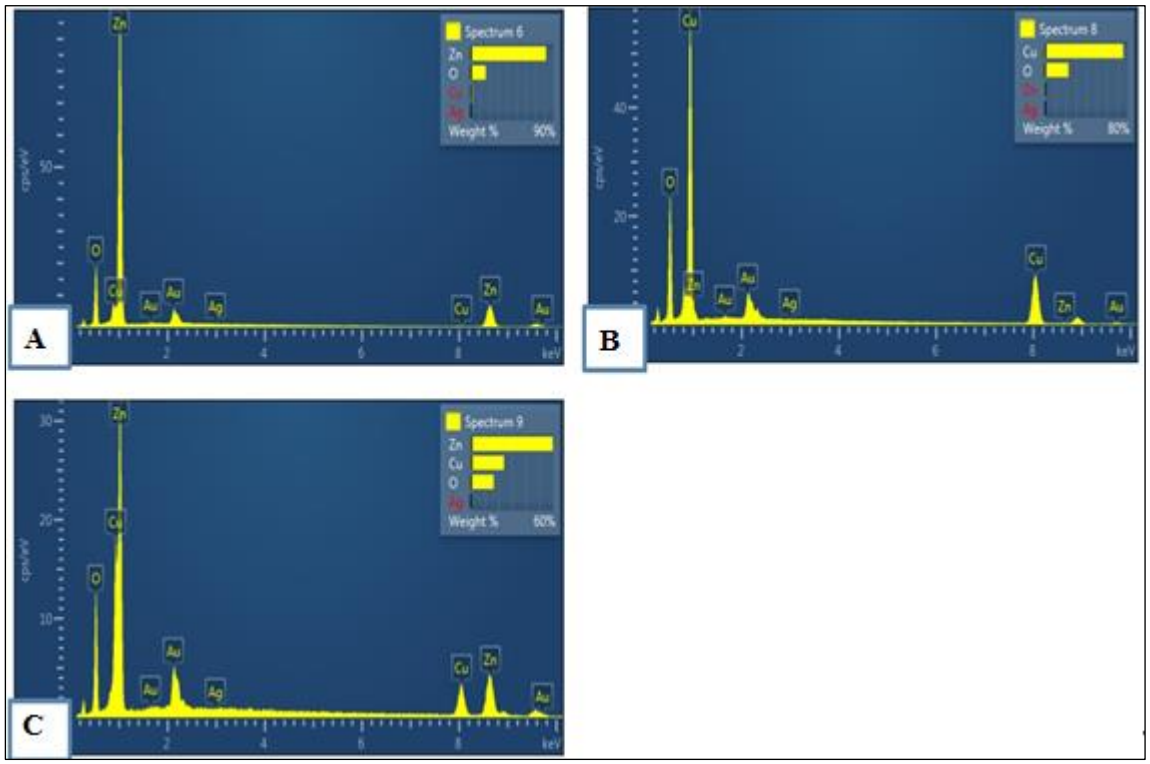

Figure 3.EDX of (**A**) ZnO NPs, (**B**) CuO NPs, (**C**) ZnO/CuO NCs.

3.4. Ultraviolet-visible (UV-Vis) analysis

UV-Vis spectroscopy was done in the range of wavelengths from 300 to 800 nm to study the optical properties of ZnO NPs, CuO NPs, and ZnO/CuO nanocomposites prepared by the green method. From **Figure 4,** the sample of ZnO NPs showed an absorbance edge at the wavelength of 300 nm, CuO NP and ZnO/CuO NCs show surface Plasmon resonance at 366 nm and 368.1 nm. This results from the interaction between incident light and free electrons in the conduction band of the nanomaterials. The location and width of the plasmon peaks depend on the size, shape, and properties of the nanowaves (27). The energy gap (E_g) was determined by graphing the correlation between photon energy ($h\upsilon$) and $(\alpha h\upsilon)^2$ utilising the Tauc method.

$$\alpha hn=A(hn-E_g)^r \quad (2)$$

The findings indicated that the energy gap for ZnO particles was approximately 4.2 eV, while for CuO, it was 3.0*8* eV ,The UV-Vis examination of the ZnO/CuO nanocomposite revealed two distinct absorption edges, indicating the different energy gaps of ZnO and CuO. The determined energy gaps were around 3.2*7* eV and 3.72 eV, respectively, indicating the influence of both ZnO and CuO phases on the optical characteristics of the composite. This outcome suggests that the nanocomposite partially preserves the optical characteristics of each constituent component. The existence of two energy gaps signifies the development of a heterojunction-like structure, which provides the composite with an expanded absorption bandwidth and improves its efficacy in photocatalytic applications and antibacterial characteristics. The prediction of the increase and change of the Eg with decreasing particle size compared to macroscopically sized semiconductors is attributed to the phenomenon of quantum confinement (28). The optical properties of nanocrystalline materials change when the size of the crystals changes (29). As we can see, the addition of CuO NPs decreases Eg; therefore, the ZnO NPs energy gap is larger than that of the ZnO/CuO composite.

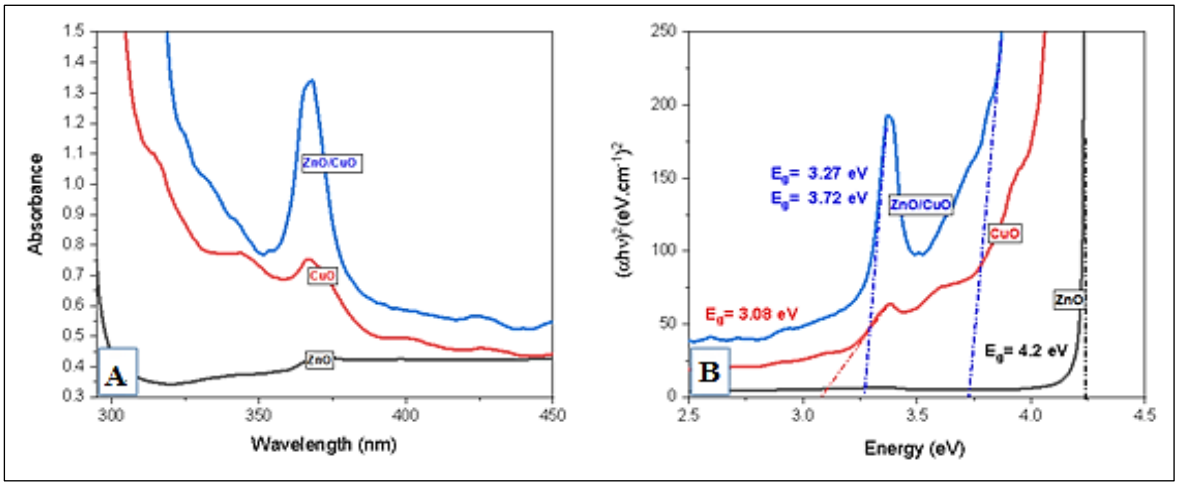

Figure 4. (**A**) UV-Vis specctrum and (**B**) Tauc plot for ZnO NPs, CuO NPs, and ZnO/CuO NCs.

3.5. FTIR Analysis

FTIR spectra of ZnO and CuO and ZnO/CuO in varying proportions in the 4000 to 500 range in **Figure 5.** FTIR was performed to identify potential biomolecules in bamboo leaf extract that are responsible for the capping, reduction, and stabilization of ZnO NPs, CuO NPs, and CuO/ZnO NPs(30). **Figure 5** shows an FTIR band located at 3441, which corresponds to O-H. It was thought that the band seen at 1643 and 1624 was caused by the C=O stretching mode in the amine I group, which is common in protein (1552), corresponding to the N-O asymmetric stretch of nitro compounds. The bands at 1151 cm^{-1} are linked to C-O, while those at 1033 cm^{-1} and 871.75 cm^{-1} are related to bending of aromatic C–H. The peaks at

594.42 and 536 cm^{-1} indicate vibrations of CuO, which confirms the creation of CuO NPs. (31). The peaks at 549 and 621 cm^{-1} are corresponding to ZnO stretching and deformation as shown in **Table 2**, respectively (32).

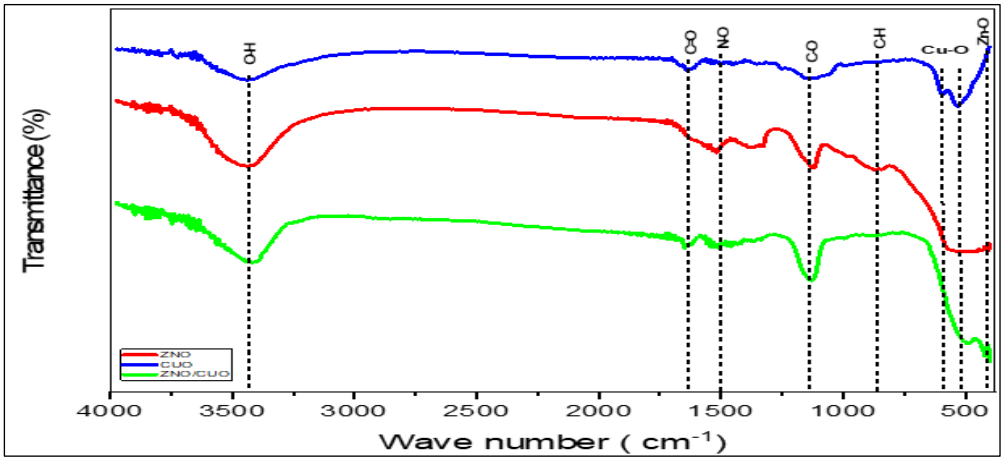

Figure 5. FTIR of synthesized ZnO NPs, CuO NPs, and ZnO/CuO NCs.

Table 2. FTIR measurements for ZnO NPs, CuO NPs, and ZnO/CuO NCs.

Band type	ZnO NPs	CuO NPs	ZnO/CuO NCs
C=O	1684	1614	1651
N–O	1526	1501	1516
C–O	1108	1151	1137
C–H	864	849	859
O–H	3410	3410	3425
ZnO	427	---	413
CuO	---	581	528, 504

3.6. Zeta potential

A zeta potential test assessed the surface charge and stability of nanomaterial particles made biologically using bamboo leaf extract. The results showed that the average zeta potential, value for ZnO NPs was +76, for CuO NPs was -57, and for the ZnO/CuO composite was +71, as illustrated in the **Figure 6.** This demonstrates the particles' exceptional stability (33).

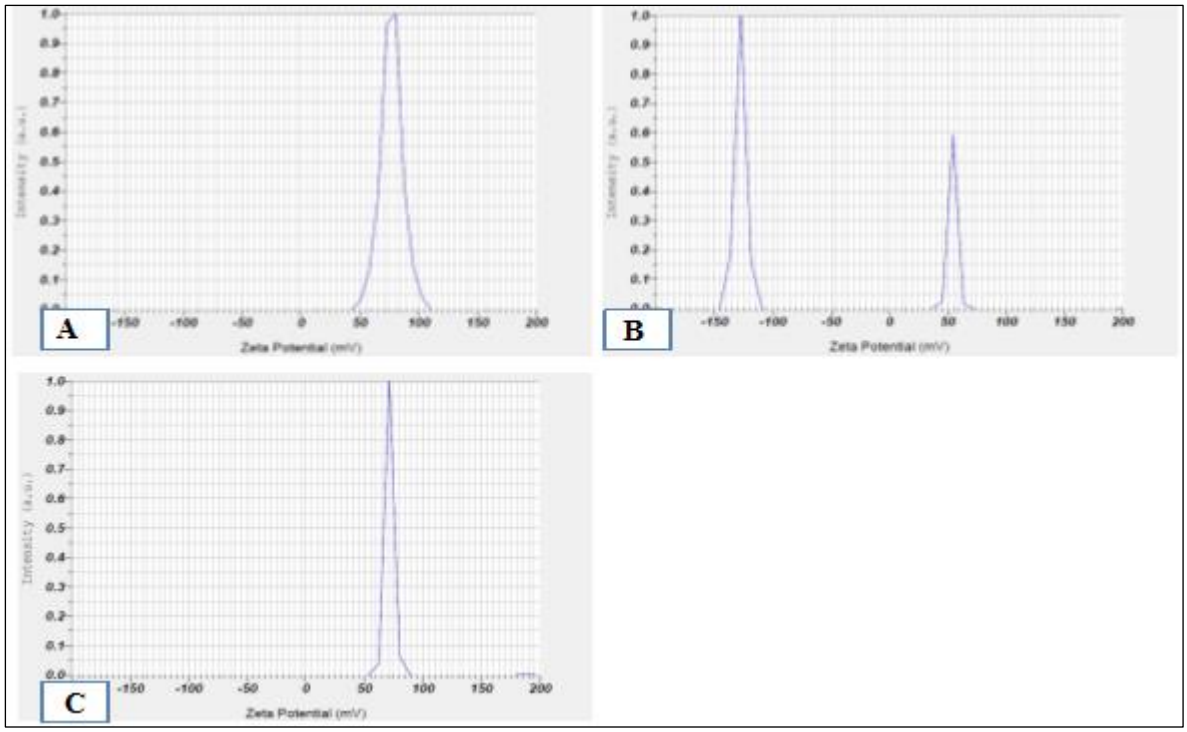

Figure 6. Zeta potential of (**A**) ZnO NPs, (**B**) CuO NPs, (**C**) ZnO/CuO NCs.

Because the strong charge inhibits agglomeration due to electrostatic repulsion, high positive and negative zeta values imply superior particle stability, while the system is less stable and there is a greater chance of particle agglomeration if the zeta value is close to zero.

3.7. Antibacterial activity

Antibacterial activity of green-synthesised CuO NPs, ZnO NPs, and ZnO/CuO CPs. The main objective of this study was to find out how well CuO NPs, ZnO NPs, and ZnO/CuO CPs work as antibacterial agents against Gram-positive and Gram-negative bacteria. Using the diffusion technique, it was selected as a test sample, ZnO, CuO, and ZnO/CuO nanoparticle suspensions were prepared by dissolving 1 g of each species in 10 mL of deionized water to obtain an original concentration of 100 mg/mL.

Different concentrations of each sample (25, 50, and 100 mg/ml) were prepared using the dilution equation ($C_1 \times V_1 = C_2 \times V_2$), where appropriate amounts of the original solution were mixed with deionized water and the **Figure 7** shows that the material shows more antibacterial activity against Gram-negative bacteria than Gram-positive bacteria, contrary to other research, including the study by (5). There is a thick layer of peptidoglycan on Gram-positive bacteria that many antibiotics can easily access (34). Gram-negative bacteria, on the other hand, have a much thinner peptidoglycan layer, surrounded by an outer membrane containing a lipopolysaccharide that many drugs cannot penetrate (35). These differences in permeability result from characteristics of the cell wall structure that determine the susceptibility of microorganisms to infection. As a result, antibiotics may find it more difficult to enter the cell, and the image also showed that the zone of inhibition expands as the concentration of nanomaterials increases.

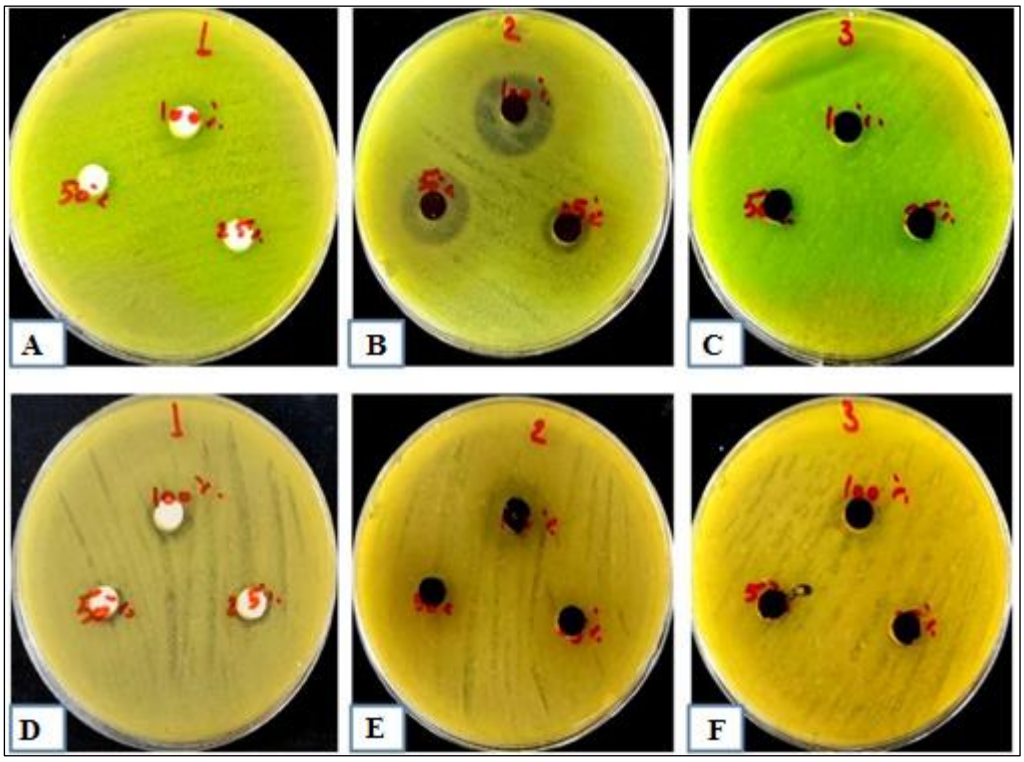

Figure 7. Antibacterial activity of (a,b) ZnO NPs (b)CuO NPs (c) ZnO/CuO NCs

Copper nanoparticles showed the widest zone of inhibition against *E. coli* at 25 millimetres. Nanoparticles adhere to bacteria, preventing them from functioning properly and damaging their outer layers that contain DNA, proteins and lipids (36). The synthesised materials were found to have excellent inhibition efficacy. This improved performance was attributed to the high content of phenolic compounds and flavonoids in bamboo leaf extract, which act as

effective reducing and stabilising agents during the synthesis process, contributing to the production of stable and highly bioactive particles. The unique shape of the particles (e.g., floral and rod shapes) as shown in FESEM analysis may enhance the surface interaction with bacterial cell membranes, thereby increasing their antibacterial efficacy. These results indicate that bamboo leaf extract is a promising and environmentally friendly option in the fabrication of multifunctional nanomaterials for medical applications. **Table 3** lists the inhibition values measured in millimetres.

Table 3. Antibacterial activity of the green synthesized ZnO NPs, CuO NPs and ZnO/CuO NCs against Gram-negative bacteria (*S.aureus*, *E coli*).

Samples	Conc. (in mg/mL)	*S. aureus* (a, c, e)	*E. coli* (b, d, f)
ZnO NPs a and b	100%	16	22
	50%	14	18
	25%	12	14
CuO NPs c and d	100%	17	25
	50%	14	18
	25%	12	14
ZnO/CuO NCs e and f	100%	17	16
	50%	15	12
	25%	13	9

4. Conclusion

In conclusion, this study demonstrates the successful green synthesis of ZnO, CuO, and ZnO/CuO nanocomposites using bamboo leaf extract as a natural reducing and stabilizing agent. The FTIR, UV-Vis, XRD, and FESEM analyses confirmed the formation of crystalline nanostructures with unique morphologies and distinct optical properties. Among the synthesized materials, CuO NPs exhibited the strongest antibacterial activity, particularly against Gram-negative E. coli, which may be attributed to its simpler cell wall structure.

Importantly, the use of bamboo leaf extract proved to be not only environmentally friendly but also more effective than other plant-based extracts reported in literature, such as neem and aloe vera, highlighting its novelty and potential as a green synthesis agent. These findings open avenues for the application of such nanomaterials in biomedical fields, especially in the development of antibacterial agents or coatings. Future studies should explore *in vivo* evaluations, long-term stability, and the mechanisms of antibacterial action to advance clinical applications.

Acknowledgment

I'd like to thank the Department of Physics at the University of Baghdad's College of Sciences for helping me finish this project by keeping private labs open and offering other scientific tools for the study project.

Conflict of Interest

Authors declare that they, have no conflict of interest.

Funding

None.

References

1. Haleem A, Javaid M, Singh RP, Rab S, Suman R. Applications of nanotechnology in medical field: a brief review. Global Health J. 2023;7(2):70–7. https://doi.org/10.1016/j.glohj.2023.02.008
2. Albrecht MA, Evans CW, Raston CL. Green chemistry and the health implications of

nanoparticles. Green Chem. 2006;8(5):417–32. https://doi.org/10.1039/B517131H
3. Gour A, Jain NK. Advances in green synthesis of nanoparticles. Artif Cells Nanomed Biotechnol. 2019;47(1):844–51. https://doi.org/10.1080/21691401.2019.1577878
4. Hayder RA, Shanan ZJ. Green synthesis and physical characterization of manganese dioxide nanoparticles using leek extract for antibacterial application. Ibn Al-Haitham J Pure Appl Sci. 2024;37(3):157–68. https://doi.org/10.30526/37.3.3503.
5. Takele E, Bogale RF, Shumi G, Kenasa G. Green synthesis, characterization, and antibacterial activity of CuO/ZnO nanocomposite using *Zingiber officinale* rhizome extract. J Chem. 2023;2023(1):3481389. https://doi.org/10.1155/2023/3481389.
6. Khan MM, Adil SF, Al-Mayouf A. Metal oxides as photocatalysts. Elsevier; 2015. p. 462–4. https://doi.org/10.1016/j.jscs.2015.04.003
7. Sharmila G, Pradeep RS, Sandiya K, Santhiya S, Muthukumaran C, Jeyanthi J. Biogenic synthesis of CuO nanoparticles using Bauhinia tomentosa leaves extract: characterization and its antibacterial application. J Mol Struct. 2018;1165:288–92. https://doi.org/10.1016/j.molstruc.2018.04.011
8. Rahman A, Harunsani MH, Tan AL, Khan MM. Zinc oxide and zinc oxide-based nanostructures: biogenic and phytogenic synthesis, properties and applications. Bioprocess Biosyst Eng. 2021;44(7):1333–72. https://doi.org/10.1007/s00449-021-02530-w.
9. El-Trass A, ElShamy H, El-Mehasseb I, El-Kemary M. CuO nanoparticles: synthesis, characterization, optical properties and interaction with amino acids. Appl Surf Sci. 2012;258(7):2997–3001. https://doi.org/10.1016/j.apsusc.2011.11.025
10. Ali A, Nasir E. Characterization of (ZnO)-(CuO)x/GaAs heterojunction solar cell grown by pulsed laser deposition. Dig J Nanomater Biostruct. 2021;16(1):169–74. https://chalcogen.ro/169_AliANM.pdf.
11. Abbas SR, Oleiwi HF. ZnO nanorod arrays for gas sensor application growing via hydrothermal technique: effect of metal oxide decoration. J Opt. 2024;1–11. https://doi.org/10.1007/s12596-024-02341-8.
12. Sharma JK, Akhtar MS, Ameen S, Srivastava P, Singh G. Green synthesis of CuO nanoparticles with leaf extract of Calotropis gigantea and its dye-sensitized solar cells applications. J Alloys Compd. 2015;632:321–5. https://doi.org/10.1016/j.jallcom.2015.01.172
13. Mousavi SB, Heris SZ. Experimental investigation of ZnO nanoparticles effects on thermophysical and tribological properties of diesel oil. Int J Hydrogen Energy. 2020;45(43):23603–14. https://doi.org/10.1016/j.ijhydene.2020.05.259
14. Chikkanna MM, Neelagund SE, Rajashekarappa KK. Green synthesis of zinc oxide nanoparticles (ZnO NPs) and their biological activity. SN Appl Sci. 2019;1(1):117. https://doi.org/10.1007/s42452-018-0095-7.
15. Desalegn T, Murthy H, Ravikumar C, Nagaswarupa H. Green synthesis of CuO nanostructures using *Syzygium guineense* (Willd.) DC plant leaf extract and their applications. J Nanostruct. 2021;11(1):81–94. https://doi.org/10.22052/JNS.2021.01.010
16. Basit RA, Abbasi Z, Hafeez M, Ahmad P, Khan J, Khandaker MU. Successive photocatalytic degradation of methylene blue by ZnO, CuO and ZnO/CuO synthesized from *Coriandrum sativum* plant extract via green synthesis technique. Crystals. 2023;13(2):281. https://doi.org/10.3390/cryst13020281
17. Ma N, Guo J, Chen S, Yuan X, Zhang T. Compositional HPLC analysis of three common bamboo leaves. Molecules. 2020;25(2):409. https://doi.org/10.3390/molecules25020409.
18. Steffy K, Shanthi G, Maroky AS, Selvakumar S. Synthesis and characterization of ZnO phytonanocomposite using *Strychnos nux-vomica* L. (Loganiaceae) and antimicrobial activity against multidrug-resistant bacterial strains from diabetic foot ulcer. J Adv Res. 2018;9:69–77. https://doi.org/10.1016/j.jare.2017.11.001.
19. Hsueh Y-H, Tsai P-H, Lin K-S. pH-dependent antimicrobial properties of copper oxide nanoparticles in *Staphylococcus aureus*. Int J Mol Sci. 2017;18(4):793. https://doi.org/10.3390/ijms18040793

20. Barzinjy AA, Hamad SM, Jalil P, Qadir R, Mirzaei Y, Shaikhah D. Green synthesis of ZnO/CuO nanocomposites using parsley extract for potential in vitro anticoccidial application. ACS Appl Bio Mater. 2023;6:–. https://doi.org/10.1021/acsabm.3c00425.
21. Patterson A. The Scherrer formula for X-ray particle size determination. Phys Rev. 1939;56(10):978. https://doi.org/10.1103/PhysRev.56.978
22. Rajesh D, Lakshmi BV, Sunandana C. Two-step synthesis and characterization of ZnO nanoparticles. Physica B. 2012;407(23):4537–9. https://doi.org/10.1016/j.physb.2012.07.050
23. Chan YB, Selvanathan V, Tey L-H, Akhtaruzzaman M, Anur FH, Djearamane S, Watanabe A, Aminuzzaman M. Effect of calcination temperature on structural, morphological and optical properties of copper oxide nanostructures derived from *Garcinia mangostana* leaf extract. Nanomaterials. 2022;12(20):3589. https://doi.org/10.3390/nano12203589 MDPI
24. Pakzad K, Alinezhad H, Nasrollahzadeh M. Green synthesis of Ni@Fe_3O_4 and CuO nanoparticles using *Euphorbia maculata* extract as photocatalysts for the degradation of organic pollutants under UV-irradiation. Ceram Int. 2019;45(14):17173–82. https://doi.org/10.1016/j.ceramint.2019.05.272.
25. Hasnidawani J, Azlina H, Norita H, Bonnia N, Ratim S, Ali E. Synthesis of ZnO nanostructures using sol-gel method. Procedia Chem. 2016;19:211–6. https://doi.org/10.1016/j.proche.2016.03.095.
26. Atri A, Echabaane M, Bouzidi A, Harabi I, Soucase BM, Chaâbane RB. Green synthesis of copper oxide nanoparticles using *Ephedra alata* plant extract and a study of their antifungal, antibacterial activity and photocatalytic performance under sunlight. Heliyon. 2023;9(2): e13484. https://doi.org/10.1016/j.heliyon.2023.e13484.
27. Paul R, Gayen R, Hussain S, Khanna V, Bhar R, Pal A. Synthesis and characterization of composite films of silver nanoparticles embedded in DLC matrix prepared by plasma CVD technique. Eur Phys J Appl Phys. 2009;47(1):10502. https://doi.org/10.1051/epjap/2009086
28. Sharma T, Patidar D, Saxena N, Sharma K. Measurement of structural and optical band gaps of $Cd_{1-x}Zn_xS$ (x = 4 and 6) nanomaterials. Indian J Pure Appl Phys. 2006; 44(2): 125-128
29. Nasir E, Alias M, Ali AM, editors. The influence of x ratio and annealing temperatures on structural and optical properties for (CuO)_x (ZnO)_1-x composite thin films prepared by PLD. IOP Conf Ser: Mater Sci Eng. 2020;757:012053. https://doi.org/10.1088/1757-899X/757/1/012053.
30. Obead AH, Abbas NK. Studying the structural and optical properties of $Zn_{1-x}Mg_xO$ nanoparticles. J Opt. 2024;1–14. https://doi.org/10.1007/s12596-024-02184-3.
31. Muslim AM, Naji IS. Green synthesis of CuO nanoparticles mediated by *Rhazya stricta* plant leaves extract: characterization and evaluation of their antibacterial and anticancer activity (*in vitro* study). Iraqi J Phys. 2024;22(3):93–105. https://doi.org/10.30723/ijp.v22i3.1259.
32. Janaki AC, Sailatha E, Gunasekaran S. Synthesis, characteristics and antimicrobial activity of ZnO nanoparticles. Spectrochim Acta A Mol Biomol Spectrosc. 2015;144:17–22. https://doi.org/10.1016/j.saa.2015.02.041.
33. Barzinjy AA, Azeez HH. Green synthesis and characterization of zinc oxide nanoparticles using *Eucalyptus globulus* leaf extract and zinc nitrate hexahydrate salt. SN Appl Sci. 2020;2(5):991. https://doi.org/10.1007/s42452-020-2813-1.
34. Naseer M, Aslam U, Khalid B, Chen B. Green route to synthesize zinc oxide nanoparticles using leaf extracts of *Cassia fistula* and *Melia azedarach* and their antibacterial potential. Sci Rep. 2020;10(1):9055. https://doi.org/10.1038/s41598-020-65949-3.
35. Nikaido H. Multidrug efflux pumps of gram-negative bacteria. J Bacteriol. 1996;178(20):5853–9. https://doi.org/10.2217/fmb.14.66.
36. Ijaz F, Shahid S, Khan SA, Ahmad W, Zaman S. Green synthesis of copper oxide nanoparticles using *Abutilon indicum* leaf extract: antimicrobial, antioxidant and photocatalytic dye degradation activities. Trop J Pharm Res. 2017;16(4):743–53. https://doi.org/10.4314/tjpr.v16i4.2.